Fabrication of SrSnO₃/rGO composite via hydrothermal technique as robust electrocatalyst for OER process

Sumia Rubab[1] · Sarah A. Alsalhi[2] · A. Dahshan[3] · Muhammad Aslam[4,5] · Khursheed Ahmad[6] ·
Albandari.W. Alrowaily[2]

Abstract

Developing effective and durable electrocatalysts for long-term energy conversion technologies is still an ongoing problem for researchers. For this purpose, perovskite oxides have attracted significant interest as effective electrocatalysts for oxygen evolution reactions (OER) in response to their highly adjustable catalytic and electrical properties associated with their compositions. This study presents a novel hydrothermal approach to fabricate SrSnO₃/rGO composite in order to accelerate the four electron transfer mechanisms. Moreover, the physical analyses show that cubic-shaped SrSnO₃ are irregularly dispersed in the form of spherical on the nanosheets of rGO. Compared with pristine, the BET study shows that composite exhibits a greater surface area ($59 \, \mathrm{m^2 \, g^{-1}}$). To evaluate the catalytic kinetics, conductivity and stability, the electrochemical evaluation of the electrode material (SrSnO₃/rGO) was performed in alkaline media with Ni foam (NF) as substrate. The exceptional electrocatalytic performance of the material in the OER could be associated with its unique structure, many active sites, and favorable conductivity. This performance is characterized by fast reaction rates, as indicated by a minimal Tafel constant ($33 \, \mathrm{mV \, dec^{-1}}$) along with reduced overpotential (199 mV) at $10 \, \mathrm{mA \, cm^{-2}}$. Moreover, the chronoamperometry (CA) investigation of the SrSnO₃/rGO composite indicates 35 h of long-term stability. This study presents a viable approach for producing high-performing perovskite composites for effective OER electrocatalysis.

Graphical Abstract
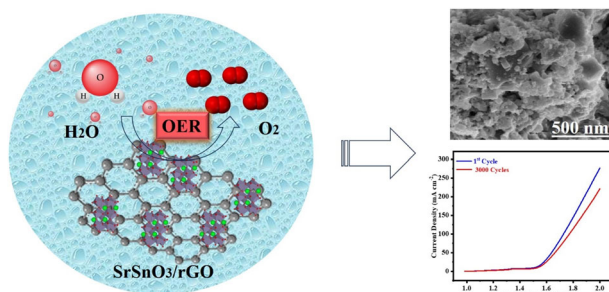
✉ Khursheed Ahmad
khursheed@yu.ac.kr

✉ Albandari.W. Alrowaily
sumiarubabbscem@gmail.com

1 Department of Chemistry, Government Graduate College Taunsa Sharif, Taunsa Sharif, Pakistan

2 Department of Physics, College of Science, Princess Nourah bint Abdulrahman University, Riyadh, Saudi Arabia

3 Department of Physics, College of Science, King Khalid University, Abha, Saudi Arabia

4 Institute of Physics and Technology, Ural Federal University, Yekaterinburg, Russia

5 Department of Physics, Gomal University, D. I. Khan, KP, Pakistan

6 School of Materials Science and Engineering, Yeungnam University, Gyeongsan, South Korea

⦻ Springer

Highlights

- The facile SrSnO$_3$/rGO nanocomposite was synthesized using a hydrothermal technique.
- The physical analysis revealed that SrSnO$_3$/rGO nanocomposite exhibit 59 m^2 g^{-1} surface area.
- The electrochemical results confirmed the fabrication of SrSnO$_3$/rGO nanocomposite with low overpotential (199 mV) and Tafel slope (33 mV dec^{-1}) at a Current density (C_d) 10 mA cm^{-2}.
- Chronoamperometry study shows that nanocomposite is highly stable for 35 h.

1 Introduction

In the early 21st century, the latest research indicates that growing global energy demand and diminishing supply of fossil fuel sources has led to substituting traditional fuels with green and environmentally friendly alternatives [1, 2] The emerging renewable energy technology, especially when coupled with irregular energy sources like the sun and wind, might significantly reduce the environmental strain caused by energy consumption [3–5]. Numerous energy conversion technologies, such as converting water molecules into high-energy molecules (e.g., oxygen or hydrogen), i.e., water splitting, are essential techniques to resolve the inherent problem of intermittency associated with these energy sources [6–8]. Nonetheless, water splitting is considered the most optimal approach for achieving this goal, and many studies have been done on this sector in recent decades [9, 10]. Water splitting comprises two partial reactions, the cathodic hydrogen evolution reaction (HER) and the anodic oxygen evolution reaction (OER) [11–16]. The 4 electrons (e$^-$) proton-associated reaction (OER) has substantial energy challenges, such as significantly lower reaction kinetics, which result in the requirement of large overpotential to proceed with the reaction [8–11]. Much research [13–17] has been done to develop effective electrocatalysts with lower overpotential and faster reaction rates by adjusting their morphological and electrical properties to perform OER [17, 18]. Among the numerous electrocatalysts produced so far, ruthenium (Ru) and iridium (Ir) based electrocatalysts have been widely used due to their greater efficiency for OER, but these electrocatalysts requires a higher overpotential (250–300 mV) and severely high cost limits their practical application [19, 20]. Comparable to precious metal oxides regarding OER activity, perovskites are a family of oxygen-containing materials with elevated OER performance owing to their greater flexibility and economical nature [21, 22]. ABO$_3$ perovskite group (A is usually a rare-earth or alkaline earth metal and B is a simple or transition metal) is of tremendous interest since it exhibits several outstanding physical features including piezoelectricity, electrochemical reactivity and ferroelectricity and chemical properties [23, 24]. The

stannate based perovskites (XSnO$_3$, where X = Sr, Ca or Ba) are a type of perovskite which has garnered significant interest due to their excellent conductivity, high durability, and enhanced electrocatalytic activity in alkaline media [9]. However, certain distinctive attributes of perovskites, such as their good catalytic activity and versatility, place them at the forefront of other widely used metal oxides, i.e., transparent conductive oxides, SnO$_2$, ZnO, and In$_2$O$_3$ [25]. Xiaomin Xu et al. introduced a collaborative co-doping approach to discover a range of BaCo$_{0.9-x}$Fe$_x$Sn$_{0.1}$O$_{3-\delta}$ perovskites with adjustable electro-catalytic efficiency for OER. By adjusting the amounts of Sn and Fe dopants, BaCo$_{0.9-x}$Fe$_x$Sn$_{0.1}$O$_{3-\delta}$ exhibits a cubical arrangement with inherent OER activity that is approximately ten times more than IrO$_2$ with Tafel value (69 mV dec^{-1}) [26]. The stable low valence of the Sr element and accessible redox potential of the Sn element, with its multivalent nature, makes SrSnO$_3$ a desirable electrocatalyst for OER.

In recent research, SrSnO$_3$ has been utilized in many applications, such as batteries and high-temperature gas sensors [27, 28]. This perovskite SrSnO$_3$ has a cubic structure at high temperatures and boasts an elevated level of combined electronic and oxygen ionic conductivity with a low overpotential [29]. Nevertheless, SrSnO$_3$ demonstrates varying polymorphs based on fabrication conditions and the cubic phase is not thermodynamically stable at ambient temperature [30]. Adding SrSnO$_3$ to a carbon-based compound, including graphene oxide (GO), carbon nanotubes, graphitic carbon nitrides (g-CN), and reduced graphene oxide (rGO) makes it more durable and improves its ability to move charges at the electrode/electrolyte contact, which results in better electrical conductivity [31]. The rGO is recognized as a conducting material on account of its enhanced surface area, superior electrical conductivity, and strong chemical endurance [32]. The coupling of perovskite with carbon (C) based compounds could enhance their OER activity due to their excellent electrical conductivity, high interfacial-to-volume ratio and superior stability [33]. Although the hydrothermal procedure reduces oxygen (O$_2$)-containing functional groups in GO, resulting in large defective regions that facilitate rapid electron transfer and the carbonyl (C=O) groups found at the corners of the GO

sheets adsorb intermediate species during the reaction, act as reactive sites for the OER [34, 35] The rGO sheets are highly conductive due to their active transfer of delocalized electrons to delocalized molecular orbitals [36, 37]. Graphene-supported catalysts consisting of non-precious metal oxides have demonstrated significant potential for OER [38, 39]. Numerous compounds of perovskite oxide have already been extremely used as photocatalysts for water splitting [40, 41]. In this regard, $SrSnO_3$ was also used as a photocatalyst in various applications [42], such as CO_2 electro reduction [36], in biological samples [43], as well as in water splitting [38] due to their spatial structure, which helps in electromobility. Hence, motivated by the above-mentioned literature, we produce an rGO-based $SrSnO_3$ composite using the hydrothermal approach, which is not yet used as an electrocatalyst for OER. The addition of rGO enhances $SrSnO_3$ surface area which helps in reducing agglomeration and promotes the charge transfer ability by providing more active sites and also induces a synergistic effect that enhances the catalytic efficiency. Moreover, $SrSnO_3$ has an outstanding electrochemical characteristic, while the rGO offers extensive surface area and superior electrical conductivity. In this regard, this combination increases charge transfer and supplies more active sites for reactions. Thus, $SrSnO_3$/rGO composites offer a viable choice for OER electrocatalysts due to their synergistic properties, enhanced stability, improved conductivity, scalable synthesis, cost-effectiveness, and lower environmental impact.

This study was done to synthesize $SrSnO_3$/rGO composite using the hydrothermal approach for OER. The analytical analyses revealed that the $SrSnO_3$ has a cubic structure, which is fully dispersed on the carbon-based structure, resulting in increased surface area ($130.44 \, m^2 \, g^{-1}$). Moreover, the electrochemical study of electrocatalysts was done using numerous electrochemical parameters. Electrochemical studies suggested that $SrSnO_3$/rGO composite exhibits low overpotential (199 mV) in obtaining C_d ($10 \, mA \, cm^{-2}$) along with Tafel value ($33 \, mV \, dec^{-1}$). This result clarifies the significance of prepared material as an electrocatalyst for OER and provides strong evidence that various methods can enhance water splitting.

2 Experimental

2.1 Reagents

Strontium carbonate ($SrCO_3$, Sigma Aldrich, 99.9%), strontium chloride ($SnCl_2$, Merck, 98%), citric acid anhydrous ($C_6H_8O_7$, AnalaR, 99%), ammonia hydroxide (NH_4OH, 31%, Sigma Aldrich), ethylene glycol ((CH_2OH)$_2$, 99%, Merck), sulphuric acid (H_2SO_4, 99%, AnalaR),

phosphoric acid (H_3PO_4, 99%, Merck), graphitic powder, potassium permanganate ($KMnO_4$, 98%, Sigma Aldrich), hydrazine solution (NH_2NH_2, 98%, AnalaR), ethanol (C_2H_5OH, 99%, Merck). Deionized water (DI) was also used in the entire fabrication method.

2.2 Preparation of $SrSnO_3$

The pure sol-gel approach was used to synthesize pure material $SrSnO_3$. To fabricate this material, 0.1 M of both precursor substances, $SrCO_3$ and $SnCl_2$, were mixed to 100 mL of ultrapure water with continuous stirring. Then, the citric acid (1.18 g), which functions as a chelating agent, was introduced into the obtained solution. To maintain the pH, 15 mL of ammonia hydroxide was poured into the obtained solution mixture drop by drop until optimum pH (9) was obtained. In the final step, ethylene glycol (5 mL) was added with constant stirring. Furthermore, the temperature was maintained at 80 °C until the water evaporated and a fine precipitate was obtained. The obtained precipitate was scraped from a beaker and collected in a crucible to annealed at 300 °C for 3 h, and finally, the annealed material was ground into fine powder.

2.3 Synthesis of rGO

Hummers' method was used to synthesize rGO using two acids, H_2SO_4 and H_3PO_4, which were mixed in a ratio of 9:1 under constant agitating for 15 min [44]. In the prepared acidic solution, 2 g of graphitic powder was incorporated at a temperature of 22 °C under continuous stirring. Moreover, the suspension of GO was obtained by adding 6 g of $KMnO_4$ in a solution with the aim of oxidizing the graphene powder. Afterward, 4 mL of H_2O_2 was inserted into a solution under steady stirring for 15 min to obtain rGO from GO and remove any residual byproduct. Furthermore, 5 mL of monohydrated hydrazine was introduced into a solution under constant agitation for 5 h. To sustain pH at 7, ultrapure water (50 mL) was mixed in a highly purified solution along with steady stirring for 15 min. The obtained mixture was cleaned multiple times with pure water and ethyl alcohol to obtain an impurities-free product. Finally, the obtained product was desiccated and preserved for further study.

2.4 Fabrication of $SrSnO_3$/rGO

The composite was prepared via a hydrothermal technique by combining 20 mg of $SrSnO_3$ and 20 mg of rGO in a 1:1 ratio in 0.03 L of water. Afterward, the prepared solution was persistently agitated for 30 min and moved to a hydrothermal reactor. After thermal treatment, the material was cooled and purified with ultrapure water and ethyl
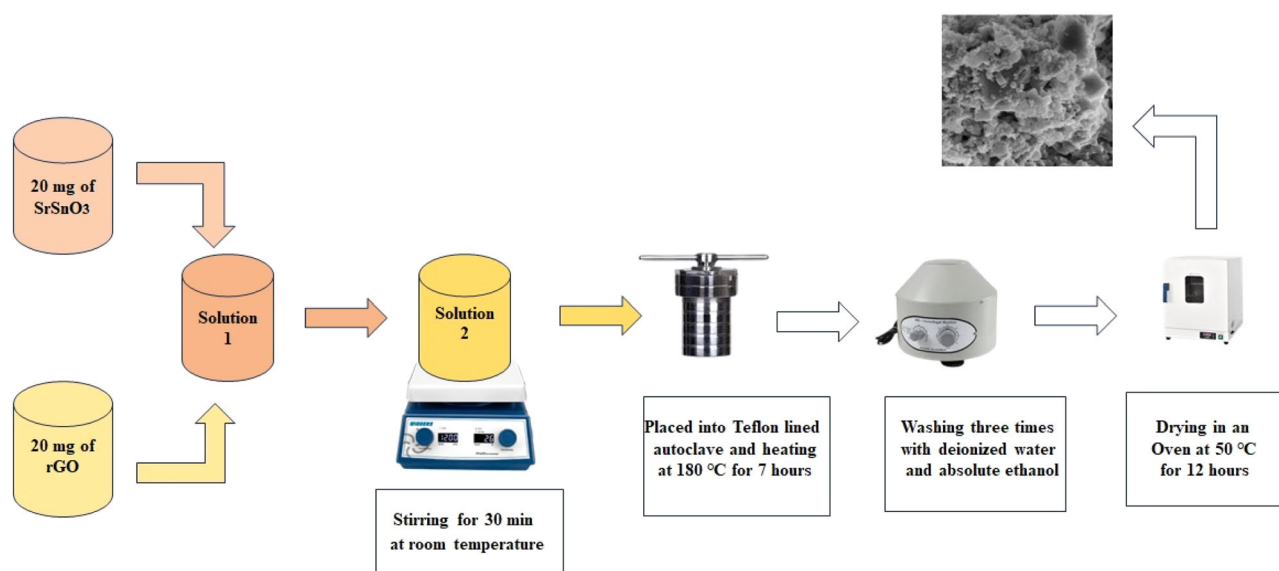
Scheme 1 The diagrammatic depiction illustrates the hydrothermal method for producing SrSnO₃/rGO composites

alcohol using centrifugation. Thus, the obtained product was dehydrated at 50 °C for 12 h. The procedure used to fabricate the SrSnO₃/rGO composite was presented in Scheme 1.

2.5 Physical measurement

An X-ray diffractometer (XRD, Bruker D-2 powder XRD) was applied to observe the crystallite structure of produced materials with a Cu-Kα source at 2θ from 10–80°. Moreover, the Raman study were acquired using a Raman microscope (MNSTEX PRI 100) equipped with a Helium and Neon laser beam source emitting light at a wavelength of 633.0 nm and a power delivery of 10 mW. The wavelength range covered was from 0 to 2000 cm⁻¹. The prepared material's morphology was analyzed with a TESCAN MIRA3 scanning electron microscope (SEM, Czech Republic). To analyze the textural properties of all prepared materials, Brunauer Emmett Teller's using N_2 as adsorbate (BET, Nova2200e Quanta chrome) was used. Moreover, the pore size distribution of all the produced material was evacuated with the Barrett–Joyner–Halenda (BJH) method (Quantchrome Autosorb iQ2).

2.6 Preparation of electrode

For the synthesis of the working electrode (WE), Ni foam was fragmented into $1 \times 1\ cm^2$ pieces and was sonicated with 5.0% HCl, acetone, ethyl alcohol, and distilled water at each stage for 15 min to eradicate the oxides' layer. Furthermore, washed NF was dehydrated in the thermal chamber for 30 min at 60 °C. The 10 mg of prepared

material was poured into 40 μL of pure water and the resultant mixture was exposed to an ultrasonic wave for 35 min. Ultimately, the resulting slurry was deposited on dry NF withg a straightforward drop caste method and desiccated for 30 min at 60 °C. The electrocatalytic efficiency of the produced material was evaluated in an alkaline solution.

2.7 Electrochemical measurement

The Metrohm AUTOLAB (PGSTAT-204) was used to investigate the electrochemical efficiency of prepared material in an alkaline media with a three-electrode workstation such as a reference electrode which is comprised of Ag/AgCl, pt wire function as auxiliary electrode, and Ni foam coated with synthesized material served as working electrode. The OER efficiency was assessed by cyclic voltammetry (CV), energy dispersive spectroscopy (EIS), chronoamperometry, and linear sweep voltammetry (LSV) using the 2.1 NOVA program. Before recording the electrochemical activity of the electrocatalyst, CV cycles at a scanning rate of 10 mV s⁻¹ were recorded to maintain their OER efficiency. However, LSV was executed with the sweeping speed (10 mV s⁻¹) at ambient temperature to test the electrocatalyst's OER efficiency and overpotentials were obtained at C_d (10 mA cm⁻²). In this research, potentials attained in the electrochemical analysis were changed to a reversible hydrogen electrode (RHE) with Eq. (1) [45].

$$E_{RHE} = E_{Ag/AgCl} + E^{\circ}_{Ag/AgCl} + 0.059pH \qquad (1)$$

The CV graph was used to quantify electro-kinetics analysis by taking the Tafel value of a linear section of the
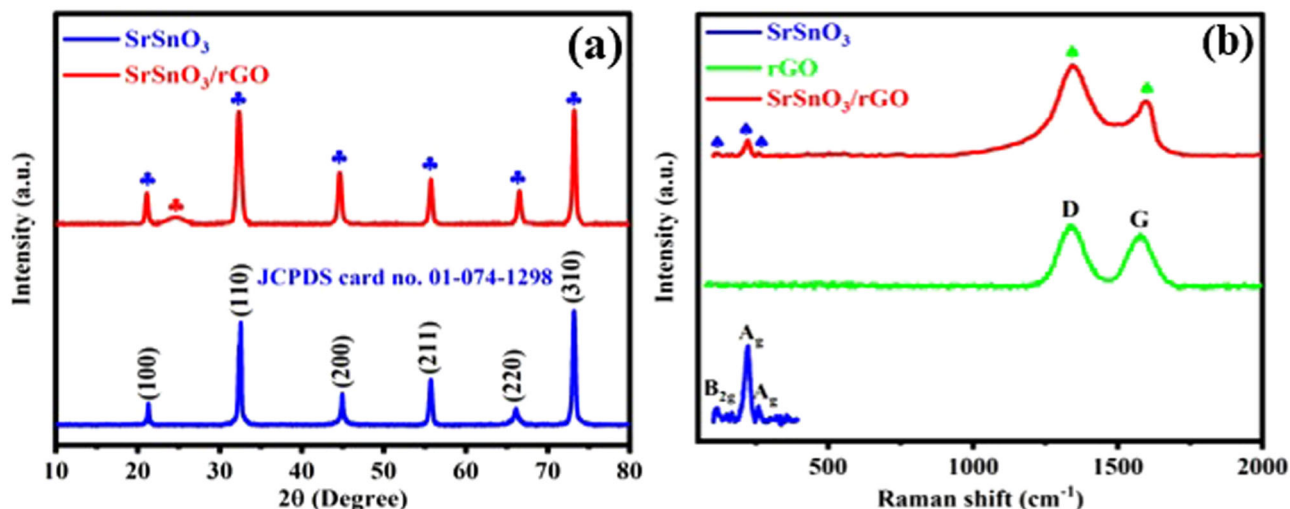
Fig. 1 a XRD Analysis and (b) Raman analysis of all prepared materials

polarization curve along with Eq. (2).

$$\eta = \alpha + \frac{2.303RT}{\alpha nF}(logj) \qquad (2)$$

The term electrochemically active surface area (ECSA) was employed to estimate the surface area of prepared material with double-layer capacitance (Cdl). As Cdl is half of the slope, it may be found by drawing the fitting line between the scanning rate and current density difference [46]. Further investigation shows that ECSA is directly proportional to Cdl and is calculated using Eq. (3).

$$ECSA = \frac{Cdl}{Cs} \qquad (3)$$

Here, C_s represents specific capacitance (0.04 mF/cm^2) [47].

$$Cdl = \frac{slope}{2} \qquad (4)$$

The roughness factor (R_f) was used to measure the electrocatalytic performance of prepared material with the equation (5).

$$R_f = \frac{ECSA}{Area} \qquad (5)$$

The factor "mass activity" is widely used to evaluate the performance of catalytic systems in proportion to active mass and electrode area. As mass activity increases, the performance of the catalyst also improves. Moreover, different factors like surface area, crystal structure, composition, and electrical properties are used to determine the mass activity of OER.

$$Mass\ activity(MA) = \frac{current\ density(j)}{Mass\ loading} \qquad (6)$$

Moreover, EIS plot was applied to evaluated the charge transfer resistance (R_{ct}) of the material and solution resistance (R_s) of the prepared material in a frequency domain of 0.1-100000 Hz. The chronoamperometry test shows the durability of the prepared material.

3 Result and discussion

3.1 Physiochemical results

The XRD analysis was accustomed to analyzing SrSnO$_3$ and SrSnO$_3$/rGO crystal structures in the 2θ range of 10–80°. Figure 1a illustrates the diffractogram of SrSnO$_3$ and SrSnO$_3$/rGO, which give 6 sharp peaks at 21.13°, 32.51°, 44.44°, 55.72°, 66.54° and 73.29° with the plane of 100, 110, 200, 211, 220 and 013, respectively. The XRD study illustrated the cubic framework of SrSnO$_3$ having parameters of a, b, and c, which are equal to 4.0254 Å, comparatively matching with JCPDS No # 01-074-1298. All of the SrSnO$_3$ peaks were present in the composite's XRD diffractogram, as shown in Fig. 1a, along with an additional peak of rGO at the 2θ range of 24.66 with plane 002 [48]. The crystallite size of pure material and composite was computed as 23.48 nm and 16.95 nm, correspondingly, using the equation named as Debye Scherer equation [49].

$$D = \frac{k\lambda}{\beta \cos\theta} \qquad (7)$$

Here, D represents crystallite size, λ is the wavelength (1.54056 nm), β represents the Full-width half maxima peaks of the pattern, and θ demonstrates the diffraction angle. As a composite's crystalline size decreases, its active sites increase, improving its electrocatalytic properties [50].
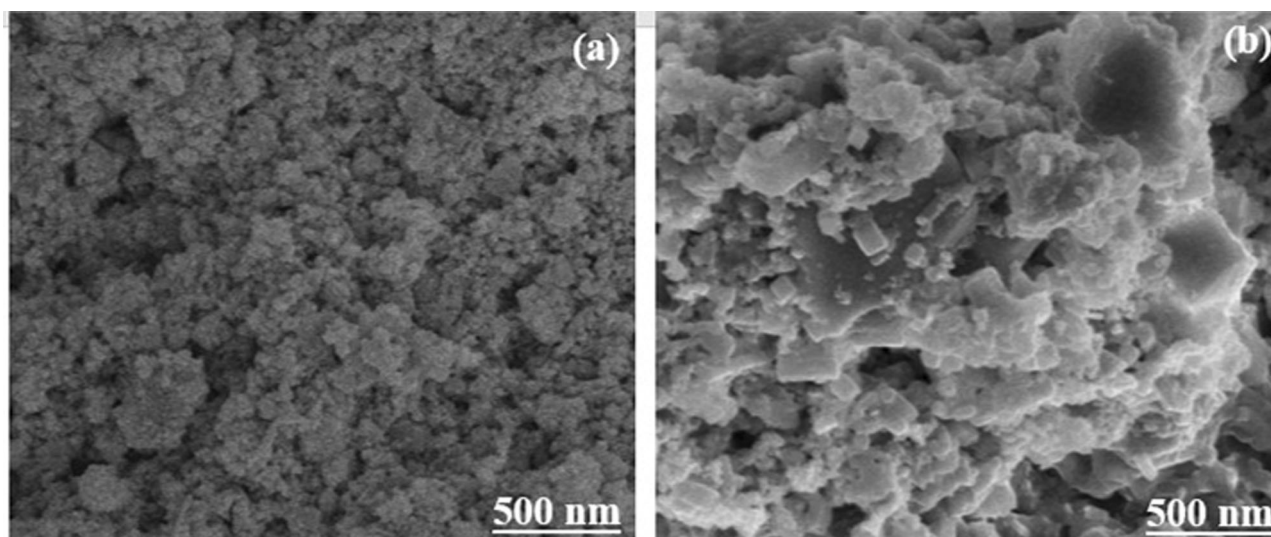
Fig. 2 SEM micrograph of (**a**) SrSnO$_3$ (**b**) SrSnO$_3$/rGO composite

Figure 1b depicted Raman spectra of pure SrSnO$_3$ and rGO-based composite SrSnO$_3$/rGO. Raman spectra of SrSnO$_3$ revealed the five vibration modes at 114, 147, 167, 223 and 259 cm^{-1} were present. From Fig. 1b, it was observed that the peaks 147 and 167 cm^{-1} correspond to A_g mode, which correlated to Sr–O–Sn and O–Sn–O bonds, correspondingly, while the other peaks at 114 relate to B_{2g} and peaks at 223, 259 relate to A_g mode which closely related with cubic structure of SrSnO$_3$ [51]. Additionally, Raman spectra of rGO revealed the existence of two bands observed at 1339 cm^{-1} and 1584 cm^{-1} that relate to the D and G band. Moreover, the D band (1339 cm^{-1}) refers to disorders and defects, particularly at the corners of graphene that occur due to the presence of heteroatoms which disrupt the crystallization of carbon belonging to A_{1g} phonons and the G band (1584 cm^{-1}) related to stretching vibration of C–C bonds in-plane which show sp^2 symmetry belong to E_g mode [38, 52]. Significantly, it has been observed that the D band exhibits high peak intensity compared to the G band. This can be attributed to the existence of a disorder on the rGO's surface that supports the SrSnO$_3$ particles [53]. Thus, the existence of all the bands of SrSnO$_3$ and rGO in the composite spectra revealed that rGO is uniformly adsorbed on the SrSnO$_3$ surface and the composite has been successfully synthesized.

The morphological analysis of all the prepared material was determined by SEM, as depicted in Fig. 2a, b. SEM microgram of SrSnO$_3$ was depicted in Fig. 2a, clearly demonstrating that the obtained material had irregularly (spherical and elongated) shaped highly dense nanoparticles. Figure 2b revealed the micrograph of SrSnO$_3$/rGO composite, demonstrating that rGO possesses a bulky sheet-like morphology. At the same time, these SrSnO$_3$ nanoparticles were uniformly dispersed on the rGO sheets,

which proved a favorable coupling of rGO and SrSnO$_3$. The dispersion of SrSnO$_3$ nanoparticles on the rGO surface was probably favorable in dealing with this association, which could eventually reduce the accumulation and restacking of the rGO sheets. It was observed that SrSnO$_3$/rGO composites could prove to be advantageous for the separation of charge carriers because of their interfacial interaction, which results in increased electrocatalytic activity [54].

The BET technique was employed to evaluate the efficacy of newly synthesized electrocatalysts by determining the textual properties of pure SrSnO$_3$ and SrSnO$_3$/rGO composite. The N$_2$ adsorption-desorption curves at 77 K were obtained for samples and the outcomes of these trends were displayed in Fig. 3a. The type IV isotherms found in adsorption/desorption isotherms with hysteresis loops (H$_4$) [55] verify the mesoporous structure of the pure and composite with surface areas of 36 and 59 m^2 g^{-1}, respectively. Based on the measured surface area values, it can be observed that SrSnO$_3$/rGO has a surface area more than SrSnO$_3$, which could potentially improve the performance of the recently developed electrocatalyst. Furthermore, the BJH technique was used to evaluate the pore volume and size of all the generated material. Meanwhile, the pore volume for SrSnO$_3$ and SrSnO$_3$/rGO composite is found to correspondingly be 22 cm^3 g^{-1} and 35 cm^3 g^{-1}, as shown in Fig. 3b. Hence, the pore size distribution validates the existence of a mesoporous structure in the materials. The porous and wide surface structure allows quick ions or electron interaction with the electrolyte, resulting in rapid faradaic redox reactions.

3.2 Electrochemical analysis

The catalytic efficiency of SrSnO$_3$ and SrSnO$_3$/rGO composite was analyzed utilizing a three-electrode workstation
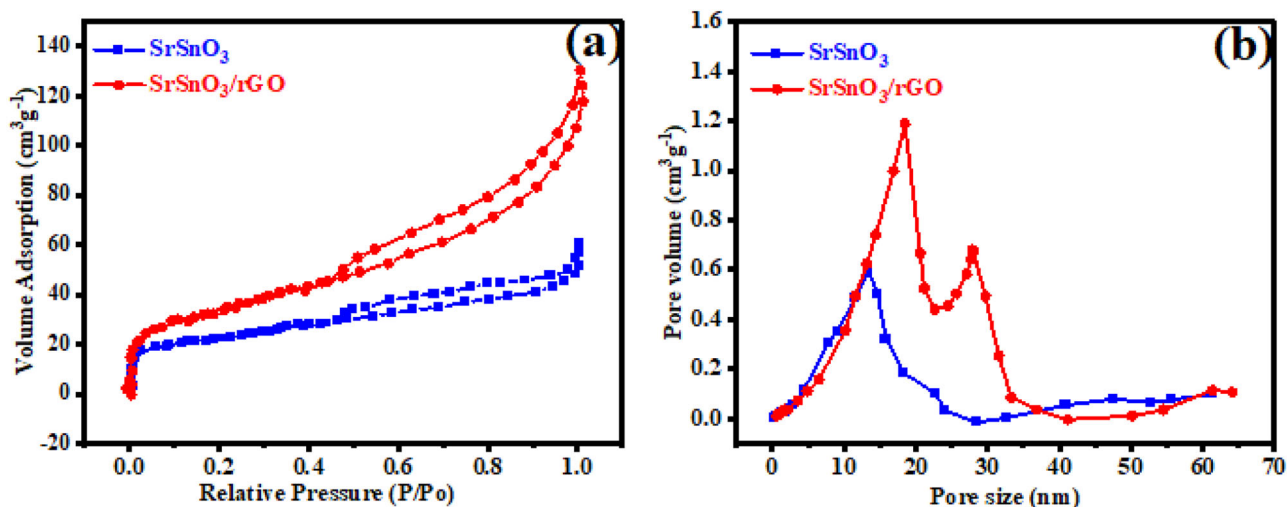
Fig. 3 a BET curves of pure SrSnO₃ material and SrSnO₃/rGO composite (**b**) pore size distribution curves of pure SrSnO₃ and SrSnO₃/rGO composite

in an alkaline media. Figure 4a, b demonstrates the CV as well as LSV curves, which illustrates the OER activity of pure and composite material at a scan speed of 10 mV s^{-1} in basic media. However, the redox behavior of SrSnO₃ and SrSnO₃/rGO was determined using a cathodic and anodic cycle of the CV curve at sweeping speed (10 mV s^{-1}) in a potential range of 0.0 to 2.0 as depicted in Fig. 4a. LSV measurements of pure and composite were taken to determine the material's catalytic efficiency, as depicted in Fig. 4b. However, the SrSnO₃/rGO's increased catalytic activity showed that the composite had a lower Tafel slope and overpotential than its pure counterpart [56]. The obtained result from the CV graph showed that the pristine SrSnO₃ and SrSnO₃/rGO composite exhibited the overpotential of 312 mV and 199 mV, respectively, as depicted in Fig. 4c. This decline in the composite overpotential was owing to its small crystalline size, diverse morphology, and more surface area, as revealed from BET analysis in Fig. 3 [1]. Figure 4d demonstrated the Tafel plot of SrSnO₃/rGO (33 mV dec^{-1}), that was significantly less than SrSnO₃ (58 mV dec^{-1}). This reduced Tafel value revealed that the reaction proceeded fast in OER with the attachment of OH$^-$ on the electrocatalyst's surface [57].

The OER procedure is thought to involve surface metal sites (Z'), which undergo a series of steps leading to an alkaline OER mechanism. First, the hydroxide anion adsorbed on the active site undergoes 1 e$^-$ (electron) oxidation, resulting in Z'–OH. After a few protons and e$^-$ removals, Z'–OH transforms into Z'–O. Following that, Z'–O will follow two distinct pathways to produce O₂ molecules. First, Z'–O decomposes into O₂ and Metal Z', while in the upcoming step, Z'–O combines with OH$^-$ to develop a Z'OOH intermediate. In the penultimate phase, Z'OOH is deprotonated to form O₂, regenerating the active

site (Table 1). The comparison of present work has been performed by already reported work is shown in Table 1.

$$Z' + OH^- \rightarrow Z'OH + e^- \tag{4}$$

$$Z'OH + OH^- \rightarrow Z'O + H_2O + e^- \tag{5}$$

$$2Z'O \rightarrow 2Z' + O_2 \tag{6}$$

$$Z'O + OH^- \rightarrow Z'OOH + e^- \tag{7}$$

$$Z'O + OH^- \rightarrow Z' + O_2 + H_2O + e^- \tag{8}$$
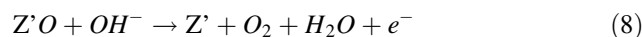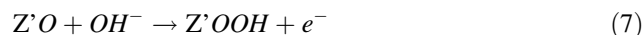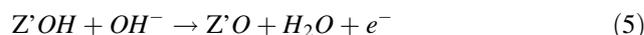
In analyzing the efficiency of electrocatalyst, especially metal oxide, for OER, it is necessary to evaluate its ECSA. As the structure of metal oxide is porous, which determines the specific surface area required for the adsorption of reactants, this adsorption capacity of reactants affects the catalytic behavior of the metal oxide. For example, a metal oxide with wider pores may have larger ECSA, as it can adsorb a greater number of reactants. The ECSA of pure and composite was evaluated in a non-faradic region of CV within the specific range (0.79–0.88 V) at different scan rate ranging from 10 to 50 mV s^{-1}, as displayed in Fig. 5a, c. Moreover, the ECSA of prepared material was determined using Cdl, which has a proportional relationship between the scan rate and the Δj in the polarization curves. Figure 5b, d illustrate that the computed Cdl value of SrSnO₃ and SrSnO₃/rGO was 8.2 mF cm^{-2} and 24.5 mF cm^{-2}, correspondingly, as estimated with Eq. 4. The higher Cdl value for the SrSnO₃/rGO composite could be attributed to the dispersion of SrSnO₃ over the surface of rGO, which produces highly defined channels that allow electrolytic ions to
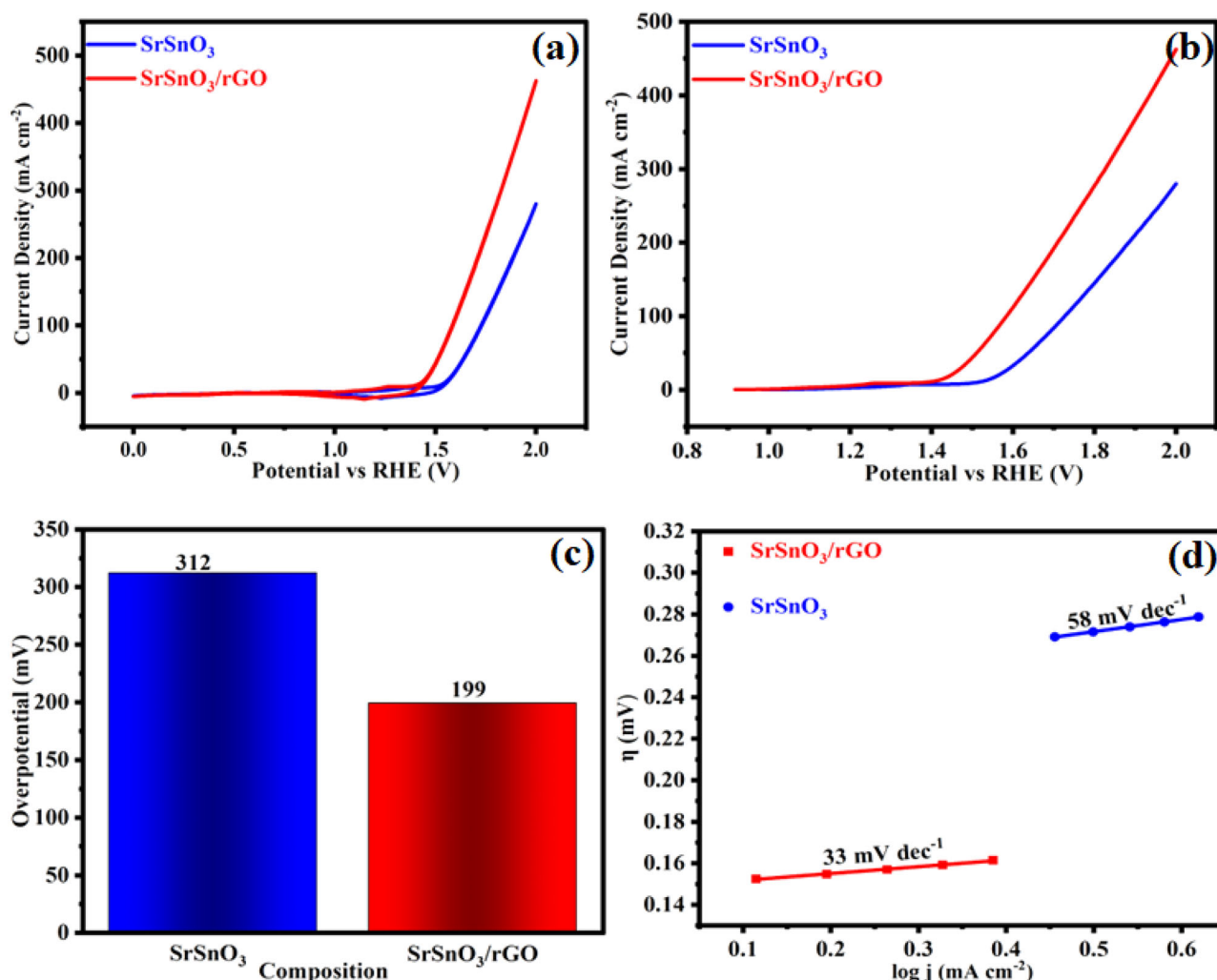
Fig. 4 a Polarization curve of prepared material (**b**) LSV curves (**c**) Overpotential of $SrSnO_3$ and $SrSnO_3$/rGO composite. **d** Tafel plot of $SrSnO_3$ and $SrSnO_3$/rGO composite

Table 1 Analyzing OER performance in relation to prepared materials and published literature

Sr. no.	Electrocatalysts	Tafel value (mV dec^{-1})	Overpotential (mV)	Electrolyte	Reference
1.	$LaCoO_3$/rGO	104	280	1.0 M KOH	[57]
2.	Fe_2O_3/rGO	115	250	1.0 M KOH	[59]
3.	Co–Fe–O/rGO	64.7	340	1.0 M KOH	[60]
4.	$La_{0.7}Sr_{0.3}CoO_3$	–	460	1.0 M KOH	[61]
5.	NiO/rGO	61	369	1.0 M KOH	[62]
6.	$NiFe_2O_4$/rGO	63	302	1.0 M KOH	[63]
7.	Co_3O_4/rGO	62	382	0.1 M KOH	[64]
8.	$Ba_{0.95}La_{0.05}FeO_3$/rGO	77	300	1.0 M NaOH	[65]
9.	Bi_2O_3-rGO	65.5	245	1.0 M KOH	[66]
10.	$SrSnO_3$/rGO	33	199	1.0 M KOH	This work

access reactive sites easily, resulting in large ECSA values [31]. The computed ECSA for $SrSnO_3$ and $SrSnO_3$/rGO composite were 205 cm^2 and 612.5 cm^2, correspondingly.

The high OER efficacy of $SrSnO_3$/rGO may be owing to numerous variables such as its high active sites, well-defined channels and large ECSA. The greater surface area
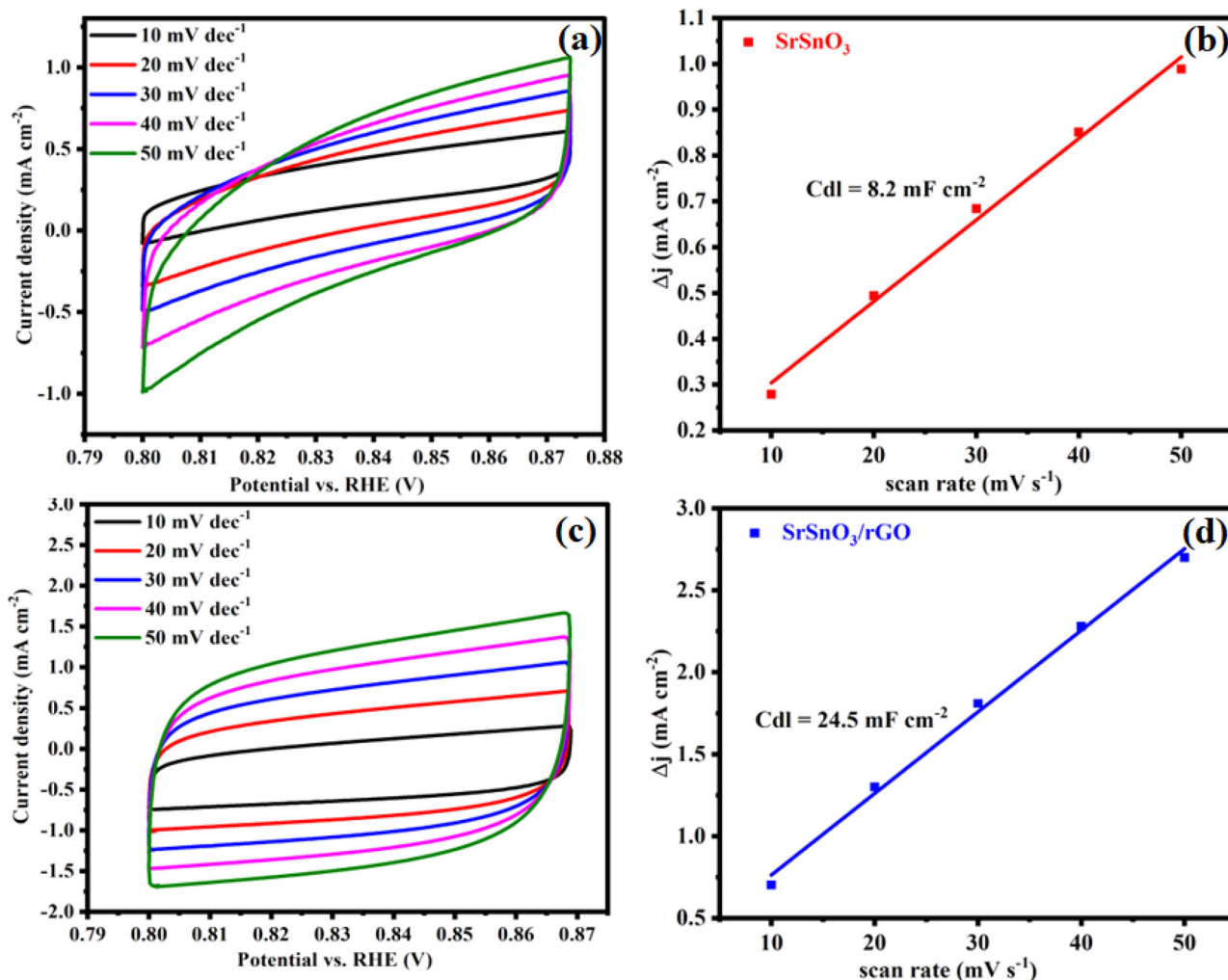
Fig. 5 a ECSA of pristine material at various scanning speeds (10–50 mV s^{-1}). **b** Cdl plot of SrSnO$_3$ (**c**) ECSA of composite material at various scanning speeds (10–50 mV s^{-1}) and (**d**) Cdl plot of SrSnO$_3$/rGO composite

results in the exposure of additional catalytic sites, leading to increased mass activity [58]. Catalysts with greater mass activity can generate a larger amount of oxygen per unit mass. This implies that a reduced amount of catalyst is necessary to attain an equivalent degree of performance, which is especially significant for enhancing resource effectiveness. The calculated R_f values of pure and composite were 410 and 1225, correspondingly. This shows that the contact area of SrSnO$_3$/rGO composite enables simple access for electrolyte ions, hence boosting the electrochemical efficiency.

The resistance of all the prepared materials can be determined by EIS in a frequency series of 0.1–100 kHz at 5 mV. The EIS plot of pristine SrSnO$_3$ and SrSnO$_3$/rGO composite gave R_s (solution resistance) and R_{ct} across electrolyte-electrode interaction, as demonstrated in Fig. 6a. The R_s value of SrSnO$_3$ and SrSnO$_3$/rGO was roughly 1.33 Ω and 1.23 Ω, and the R_{ct} of SrSnO$_3$ and SrSnO$_3$/rGO composite was around 3.69 Ω and 0.16 Ω, correspondingly.

This decline in R_{ct} and R_s values for composite compared to the pristine results in the increased conductivity of the material and the fast dynamics of OER. Moreover, the chronoamperometry stability tests was applied to assess the durability of the composite, which was used as an electrocatalyst during water splitting, as displayed in Fig. 6b. The chronoamperometry of the composite demonstrated that at the first 10 h, the current density of SrSnO$_3$/rGO indicated a little drop and then remained enduring for 35 h at C$_d$ of 67 mA cm^{-2}. The LSV stability experiment was conducted to assess the durability of the composite at 10 mV s^{-1} for 3000th cycles during OER, as depicted in Fig. 6c. Furthermore, the LSV curve of the first SrSnO$_3$/rGO composite cycle was analogous to the 3000th one. After 3000th cycles of stability tests, the LSV curve demonstrated that the composite exhibited excellent stability during the water oxidation reaction with a slight reduction in current density. Thus, no obvious shifts were detected in the LSV peak of SrSnO$_3$/rGO composite after the 3000th cycle.
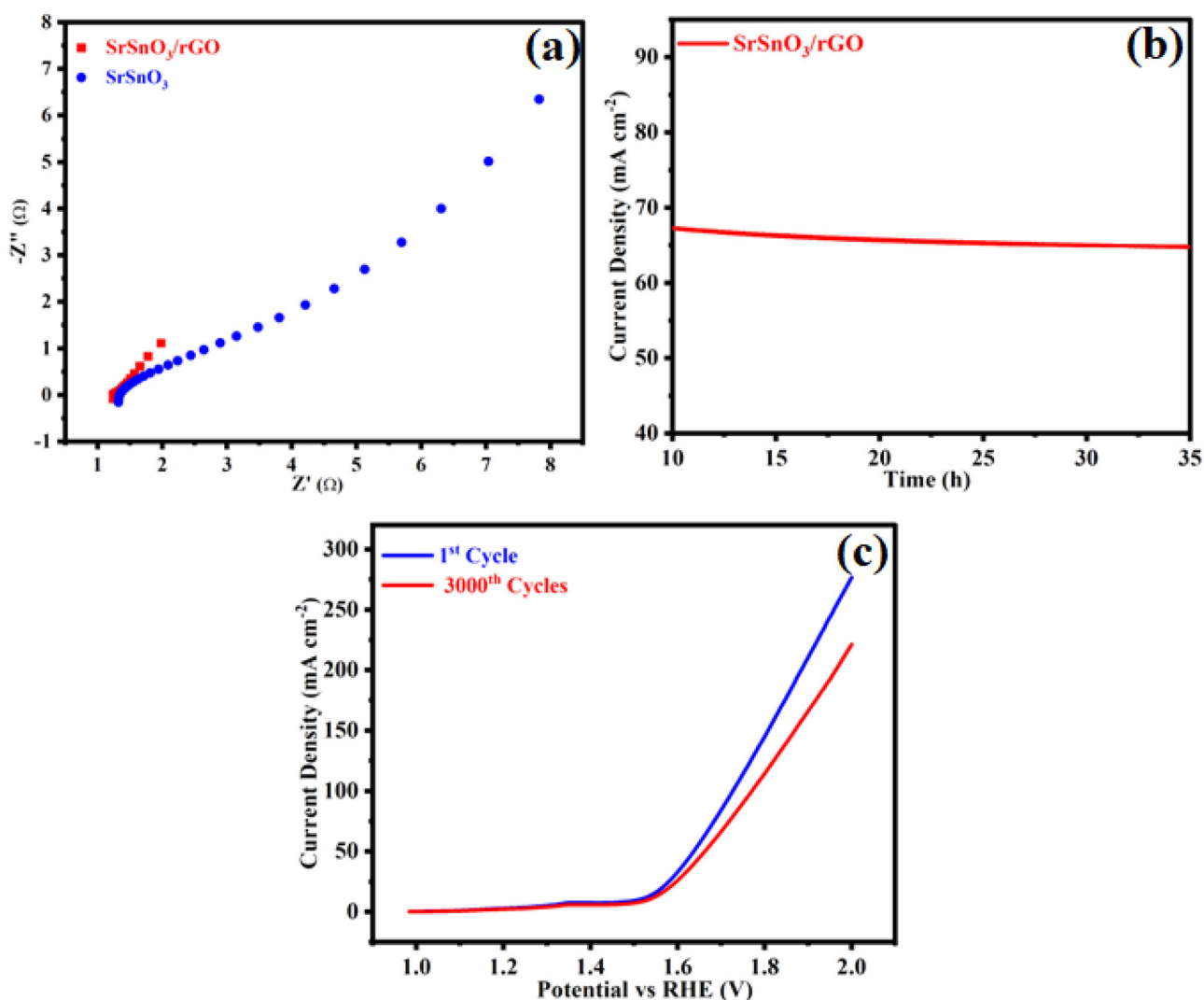
Fig. 6 a EIS of $SrSnO_3$ and $SrSnO_3$/rGO composite. **b** Chronoamperometry (CA) of $SrSnO_3$/rGO composite. **c** LSV stability of $SrSnO_3$/rGO composite

4 Conclusion

This investigation presents a new hydrothermal method to fabricate the $SrSnO_3$/rGO composite, which functioned as an effective electrocatalyst for the OER. The Physical characterizations were used to evaluate the produced materials' morphology, textual properties, and structure. The analysis found that the rGO-based $SrSnO_3$ composite had an overpotential of 199 mV, resulting in a C_d of around ~10 mA cm^{-2} and a Tafel gradient (33 mV dec^{-1}). The electrocatalytic activity of $SrSnO_3$/rGO composite was validated by EIS and chronoamperometry study, demonstrating high conductivity assigned to the expanded surface area confirmed by cubic structure and stability for 35 h. This present research shows a novel strategy for increasing the performance of stannate-based catalysts by employing rGO

as an appropriate material for producing several active sites. The prepared composite serves as a competent electrode material for OER performance and offers new possibilities for various applications.

Compliance with ethical standards

Conflict of interest The authors declare no competing interests.

References

1. Alwadai N, Manzoor S, Al Huwayz M, Abdullah M, Khosa RY, Aman S, Abid AG, Alrowaili ZA, Al-Buriahi MS, Farid HMT (2023) Facile synthesis of transition metal oxide SnO2/MnO2 hierarchical nanostructure: as an efficient electrocatalyst for robust oxygen evolution reaction. Surf Interfaces 36:102467. https://doi.org/10.1016/J.SURFIN.2022.102467

2. Rasool N, Alqarni AS, Ahmad K, Al-Sehemi AG, Henaish AMA, Aman S (2024) Enhancement of BaCeO3 OER performance by generating a nanohybrid with gCN for electrochemical water splitting. International J Hydrog Energy 81:562–572, ISSN 0360–3199, https://doi.org/10.1016/j.ijhydene.2024.07.132

3. Hussain M, Maaty El LA, Alomar MA, Ali M, Abdullah M, Aman S, Farid HMT (2024) Ahmad I Improvement of spinel OER electrochemical property by doping strategy for water splitting. Appl. Phys. A 130:554. https://doi.org/10.1007/s00339-024-07679-1

4. Gouadria S, Abudllah M, Ahmad Z, John P, Nisa MU, Manzoor S, Aman S, Ashiq MN, Ghori MI (2023) Development of bifunctional Mo doped ZnAl2O4 spinel nanorods array directly grown on carbon fiber for supercapacitor and OER application. Ceram Int 49:4281–4289. https://doi.org/10.1016/J.CERAMINT.2022.09.312

5. Liu PF, Yin H, Fu HQ, Zu MY, Yang HG, Zhao H (2020) Activation strategies of water-splitting electrocatalysts. J Mater Chem A 8:10096–10129. https://doi.org/10.1039/D0TA01680B

6. Alharbi FF, Alahmari SD, Aman S, Dahshan A, Henaish AMA (2024) Developing TiCo2O4 spinel based on rGO nanosheet to enhance electrochemical performance of OER activity. Journal of Electroanalytical Chemistry, 963:118299, https://doi.org/10.1016/j.jelechem.2024.118299.

7. Alharbi FF, Zulfiqar M, Ejaz SR, Aman S, Aslam M, Abdullah M, Al-Sehemi AG, Henaish AMA, Ahmad K, Farid HMT (2024) Effect of Mn dopant on physiochemical properties of V2O5 and their photocatalytic application toward mineralization of malachite green (MG) dye, Materials Chemistry and Physics, 322:129556, https://doi.org/10.1016/j.matchemphys.2024.129556.

8. Wang Y, Kong B, Zhao D, Wang H, Selomulya C (2017) Strategies for developing transition metal phosphides as heterogeneous electrocatalysts for water splitting. Nano Today 15:26–55. https://doi.org/10.1016/J.NANTOD.2017.06.006

9. Alharbi FF, Aman S, Abdullah M, Abid AG, Manzoor S, Khosa RY, Farid HMT, Silibin MV, Trukhanov S.V, Zubar TI, Trukhanov AV (2024) Development of Mn doped ZnAl2O4 via hydrothermal method as photocatalyst for Cr(VI) reduction under visible light, Ceramics International. 50:24177–24185. https://doi.org/10.1016/j.ceramint.2024.04.149

10. Khan NA, Rashid N, Junaid M, Zafar MN, Faheem M, Ahmad I (2019) NiO/NiS heterostructures: an efficient and stable electrocatalyst for oxygen evolution reaction. ACS Appl Energy Mater 2:3587–3594. https://doi.org/10.1021/ACSAEM.9B00317/SUPPL_FILE/AE9B00317_SI_001.PDF

11. She ZW, Kibsgaard J, Dickens CF, Chorkendorff I, Nørskov JK, Jaramillo TF (2017) Combining theory and experiment in electrocatalysis: insights into materials design. Science. 355. https://doi.org/10.1126/SCIENCE.AAD4998.

12. Manzoor S, Trukhanov SV, Ansari MN, Abdullah M, Alruwaili A, Trukhanov AV, Khandaker MU, Idris AM, El-Nasser KS, Taha TA(2022) Flowery ln2MnSe4 novel electrocatalyst developed via anion exchange strategy for efficient water splitting Nanomaterials 12:2209. https://doi.org/10.3390/NANO12132209

13. Alburaih HA, Manzoor S, Abdullah M, Ashiq MN, Aman S, Trukhanov SV, Zubar TI, Sun Z, Taha TA, Trukhanov AV (2023) Electro-oxidation reconstitution of aluminium copper MOF-derived metal oxyhydroxides for a robust OER process. RSC Adv 13:8736–8742. https://doi.org/10.1039/D2RA07661F

14. Hunter BM, Thompson NB, Mü AM, Rossman GR, Hill MG, Winkler JR, Gray HB (2018) A.M. Mü Ller, Trapping an iron(VI) water-splitting intermediate in nonaqueous media. Joule 2:747–763. https://doi.org/10.1016/j.joule.2018.01.008

15. Suntivich J, May KJ, Gasteiger HA, Goodenough JB, Shao-Horn Y (2011) A perovskite oxide optimized for oxygen evolution catalysis from molecular orbital principles. Science 334:1383–1385. https://doi.org/10.1126/SCIENCE.1212858

16. Aman S, Gouadria S, Manzoor S, Abdullah M, Khosa RY, Ashiq MN, Ansari MZ, Alfantazi A (2023) Facile synthesis of CuZrO3@PPY nanohybrid balls embedded 3-dimensional network with synergistic effect for efficient oxygen evolution reaction. Surf Interfaces 36:102607. https://doi.org/10.1016/J.SURFIN.2022.102607

17. Li Y, Hu L, Zheng W, Peng X, Liu M, Chu PK, Yoon L, Lee S (2018) Communication Ni/Co-based nanosheet arrays for efficient oxygen evolution reaction. Nano Energy 52:360–368. https://doi.org/10.1016/j.nanoen.2018.08.010

18. Alharbi FF, Aman S, Ahmad N, Abdullah M, Abid AG, Manzoor S, Trukhanov S, Sayyed MI, Tishkevich D, Trukhanov A (2023) Investigation of photoreduction of Cr (VI) and electrocatalytic properties of hydrothermally produced novel CoFe2O4/ZnO nanostructure. Solid State Sci 143:107278. https://doi.org/10.1016/J.SOLIDSTATESCIENCES.2023.107278

19. Alanazi MM, Abdelmohsen SAM, Alahmari SD, Abdullah M, Aman S, Al-Sehemi AG Farid HMT (2024) Development of magnetically separable MoS2/NiFe2O4 heterostructure for improved photocatalytic efficiency of malachite green (MG) degradation. J Mater Sci: Mater Electron 35:1045. https://doi.org/10.1007/s10854-024-12778-z

20. Stoerzinger KA, Rao RR, Wang XR, Hong WT, Rouleau CM, Shao-Horn Y (2017) The role of Ru redox in pH-dependent oxygen evolution on rutile ruthenium dioxide surfaces. Chem 2:668–675. https://doi.org/10.1016/J.CHEMPR.2017.04.001

21. Li BQ, Xia ZJ, Zhang B, Tang C, Wang HF, Zhang Q (2017) Regulating p-block metals in perovskite nanodots for efficient electrocatalytic water oxidation Nat Commun 8:1–7. https://doi.org/10.1038/s41467-017-01053-x

22. Nisa MU, Manzoor S, Abid AG, Tamam N, Abdullah M, Najam-Ul-Haq M, Al-Buriahi MS, Alrowaili ZA, Mahmoud ZMM, Ashiq MN (2022) CdSe supported SnO2 nanocomposite with strongly hydrophilic surface for enhanced overall water splitting. Fuel 321:124086. https://doi.org/10.1016/J.FUEL.2022.124086

23. Liu Q, Jin F, Li B, Geng L (2017) Structure and band gap energy of CaSnO3 epitaxial films on LaAlO3 substrate. J Alloy Compd 717:55–61. https://doi.org/10.1016/J.JALLCOM.2017.05.112

24. Zahra T, Alotaibi BM, Alrowaily AW, Alyousef HA, Al-Sehemi AG, Aman S (2024) Boosting the energy-storing performance of hydrothermally synthesized ZnO by MnTe for supercapacitor applications. J Mater Sci: Mater Electron 35:1086. https://doi.org/10.1007/s10854-024-12807-x

25. James KK, Krishnaprasad PS, Hasna K, Jayaraj MK (2015) Structural and optical properties of La-doped BaSnO3 thin films grown by PLD. J Phys Chem Solids 76:64–69. https://doi.org/10.1016/J.JPCS.2014.07.024

26. Xu X, Su C, Zhou W, Zhu Y, Chen Y, Shao Z, Xu X, Zhou W, Zhu Y, Chen Y, Su C, Shao Z (2016) Co-doping strategy for developing perovskite oxides as highly efficient electrocatalysts for oxygen evolution reaction. Adv Sci 3:1500187. https://doi.org/10.1002/ADVS.201500187

27. Wang B, Zhang W, Yang K, Liao T, Li F, Cui Y, Gao Y, Liu B (2018) Metal dopants adjusted perovskite stannates: conductivity and optical properties. Ceram Int 44:16051–16057. https://doi.org/10.1016/J.CERAMINT.2018.06.046

28. Hussain M, Alanazi MM, Abdelmohsen SAM, Abdullah M, Ali M, Aman S, Al-Sehemi AG, Henaish AM, Farid HM (2024) Enhanced Supercapacitive Performance of FeAl2O4 Nanoparticles with Neodymium (Nd) Doping by Sonication Method. JOM 76:3185–3194. https://doi.org/10.1007/s11837-024-06518-1

29. Hussain M, El Maati LA, Alomar MA, Ali M, Abdullah M, Aman S, Farid HMT (2024) Improvement of SnFe2O4 OER electrochemical property by Sm doping for water splitting. Ceramics International, 50:19525–19533, https://doi.org/10.1016/j.ceramint.2024.03.050

30. Wang T, Prakash A, Dong Y, Truttmann T, Bucsek A, James R, Fong DD, Kim JW, Ryan PJ, Zhou H, Birol T, Jalan B (2018) Engineering SrSnO3 phases and electron mobility at room temperature using epitaxial strain. ACS Appl Mater Interfaces 10:43802–43808. https://doi.org/10.1021/ACSAMI.8B16592/SUPPL_FILE/AM8B16592_SI_001.PDF

31. Manzoor S, Nisa MU, Abid AG, Abdullah M, Mersal GAM, Ibrahim MM, Taha Hamida TAM, Ashiq MN (2022) SnTe nanomaterial decorated over graphene nanosheet for robust OER activity. Int J Energy Res 46:24622–24632. https://doi.org/10.1002/ER.8685

32. Salarizadeh P, Askari MB, Di A (2022) Bartolomeo, MoS2/Ni3S2/reduced graphene oxide nanostructure as an electrocatalyst for alcohol. Fuel Cells ACS Appl Nano Mater 5:3361–3373. https://doi.org/10.1021/ACSANM.1C03946/ASSET/IMAGES/LARGE/AN1C03946_0010.JPEG

33. Askari MB, Salarizadeh P, Beheshti-Marnani A (2020) A hierarchical hybrid of ZnCo2O4 and rGO as a significant electrocatalyst for methanol oxidation reaction: synthesis, characterization, and electrocatalytic performance. Int J Energy Res 44:8892–8903. https://doi.org/10.1002/ER.5597

34. Askari MB, Salarizadeh P, Di Bartolomeo A, Şen F (2021) Enhanced electrochemical performance of MnNi2O4/rGO nanocomposite as pseudocapacitor electrode material and methanol electro-oxidation catalyst. Nanotechnology 32:325707. https://doi.org/10.1088/1361-6528/ABFDED

35. Askari MB, Salarizadeh P, Beheshti-Marnani A, Di Bartolomeo A (2021) NiO-Co3O4-rGO as an efficient electrode material for supercapacitors and direct alcoholic fuel cells. Adv Mater Interfaces 8:2100149. https://doi.org/10.1002/ADMI.202100149

36. Aman S, Farid HMT, Manzoor S, Ashiq MN, Khosa RY, Elsayed KA, Mahmoud KH, Taha TA, Waheed MS, Abdullah M (2022) High performance graphene oxide/NiAl2O4 directly grown on carbon cloth hybrid for oxygen evolution reaction. Int J Hydrogen Energy 47:34299–34311. https://doi.org/10.1016/J.IJHYDENE.2022.08.033

37. Yang A, Li T, Jiang S, Wang X, Qiu X, Lei W, Tang Y (2019) High-density growth of ultrafine PdIr nanowires on graphene: reducing the graphene wrinkles and serving as efficient bifunctional electrocatalysts for water splitting. Nanoscale 11:14561–14568. https://doi.org/10.1039/C9NR03027A

38. Nagaraju G, Manjunath K, Sarkar S, Gunter E, Teixeira SR, Dupont J (2015) TiO2–RGO hybrid nanomaterials for enhanced water splitting reaction. Int J Hydrogen Energy 40:12209–12216. https://doi.org/10.1016/J.IJHYDENE.2015.07.094

39. Manzoor S, Alsaiari NS, Katubi KM, Nisa MU, Abid AG, Chughtai AH, Abdullah M, Aman S, Al-Buriahi MS, Ashiq MN (2023) Facile fabrication of SnSe nanorods embedded in GO nanosheet for robust oxygen evolution reaction. J Taibah Univ Sci 17:2151298. https://doi.org/10.1080/16583655.2022.2151298

40. Suzuki S, Iwase A, Kudo A (2020) Long wavelength visible light-responsive SrTiO3 photocatalysts doped with valence-controlled Ru for sacrificial H2 and O2 evolution. Catal Sci Technol 10:4912–4916. https://doi.org/10.1039/D0CY00600A

41. Li Y, Gou H, Lu J, Wang C (2014) A two-step synthesis of NaTaO3 microspheres for photocatalytic water splitting. Int J Hydrogen Energy 39:13481–13485. https://doi.org/10.1016/J.IJHYDENE.2014.03.023

42. Alahmari SD, Alsalhi SA, Abdullah M, Al-Sehemi AG, Henaish AMA, Ahmad Z, Aman S (2024) Development of Mn doped CeTe as an environmental purifier for photodegradation of noxious methylene blue dye in water. Journal of Physics and Chemistry of Solids, 188:111909. https://doi.org/10.1016/j.jpcs.2024.111909.

43. Zahra T, Alanazi MM, Abdelmohsen SAM, Alahmari SD, Abdullah M, Aman S, Dahshan A, Henaish AMA, Ahmad Z, Farid HMT (2024) Fabrication of MnAl2O4/g-CN nanohybrid as an advantageous electrode for supercapacitor applications. Ceramics International, 50:14469–14479. https://doi.org/10.1016/j.ceramint.2024.01.359.

44. Shao D, Li P, Zhang R, Zhao C, Wang D, Zhao C (2019) One-step preparation of Fe-doped Ni3S2/rGO@NF electrode and its superior OER performances. Int J Hydrogen Energy 44:2664–2674. https://doi.org/10.1016/J.IJHYDENE.2018.11.054

45. Lei S, Li QH, Kang Y, Gu ZG, Zhang J (2019) Epitaxial growth of oriented prussian blue analogue derived well-aligned CoFe2O4 thin film for efficient oxygen evolution reaction. Appl Catal B Environ 245:1–9. https://doi.org/10.1016/J.APCATB.2018.12.036

46. Prasad K, Sreekanth TVM, Yoo K, Kim J (2023) Surfactant-assisted hydrothermal synthesis of CoFe2O4 nanostructures and their application in the oxygen evolution reaction. Mater Lett 349:134859. https://doi.org/10.1016/J.MATLET.2023.134859

47. Prasad K, Sreekanth TVM, Yoo K, Kim J (2024) Facile synthesis of nanostructured MnCo2O4.5 with spheres and puffed rice balls-like structures as high-performance electrocatalysts for oxygen evolution reaction. Mater Lett 368:136696. https://doi.org/10.1016/J.MATLET.2024.136696

48. Ikram M, Raza A, Imran M, Ul-Hamid A, Shahbaz A, Ali S (2020) Hydrothermal synthesis of silver decorated reduced graphene oxide (rGO) nanoflakes with effective photocatalytic activity for wastewater treatment. Nanoscale Res Lett 15:1–11. https://doi.org/10.1186/S11671-020-03323-Y/FIGURES/9

49. Abdullah M, John P, Ashiq MN, Manzoor S, Ghori MI, Nisa MU, Abid AG, Butt KY, Ahmed S (2023) Development of CuO/CuS/MnO2 ternary nanocomposite for visible light-induced photocatalytic degradation of methylene blue Nanotechnol Environ Eng 8:63–73. https://doi.org/10.1007/S41204-022-00266-W/METRICS

50. Ardizzone S, Bianchi CL, Cappelletti G, Ionita M, Minguzzi A, Rondinini S, Vertova A (2006) Composite ternary SnO2–IrO2–Ta2O5 oxide electrocatalysts. J Electroanal Chem 589:160–166. https://doi.org/10.1016/J.JELECHEM.2006.02.004

51. Pérez Hernández CG, Flores-Pacheco A, Carrillo Torres RC, Carrera AA, Zeferino RS, Enrique M, Ramos Á (2018) Structural and luminescent properties of samarium doped SrSnCb nanoparticles. Microsc Microanal 24:1746–1747. https://doi.org/10.1017/S1431927618009212

52. Jiang G, Lin Z, Chen C, Zhu L, Chang Q, Wang N, Wei W, Tang H (2011) TiO2 nanoparticles assembled on graphene oxide nanosheets with high photocatalytic activity for removal of pollutants. Carbon 49:2693–2701. https://doi.org/10.1016/J.CARBON.2011.02.059

53. Madakannu I, Patil I, Kakade BA, Kasibhatta KRD (2020) Boosting oxygen evolution reaction performance by nickel substituted cobalt-iron oxide nanoparticles embedded over reduced graphene oxide. Mater Chem Phys 252:123238. https://doi.org/10.1016/J.MATCHEMPHYS.2020.123238

54. Venkatesh G, Geerthana M, Prabhu S, Ramesh R, Prabu KM (2020) Enhanced photocatalytic activity of reduced graphene oxide/SrSnO3 nanocomposite for aqueous organic pollutant

degradation. Optics 206:164055. https://doi.org/10.1016/J.IJLEO.2019.164055

55. Fan Z, Liao F, Shi H, Liu Y, Shao M, Kang Z (2020) Highly efficient water splitting over a RuO2/F-doped graphene electrocatalyst with ultra-low ruthenium content. Inorg Chem Front 7:2188–2194. https://doi.org/10.1039/D0QI00095G

56. Sadaqat M, Manzoor S, Aman S, Nisar L, Najam-Ul-Haq M, Shah A, Shawky AM, Ali HE, Ashiq MN, Taha TA (2023) Defective nickel zirconium oxide mesoporous bifunctional electrocatalyst for oxygen evolution reaction and overall water splitting, Fuel, 333:126538, https://doi.org/10.1016/j.fuel.2022.126538

57. Ahmed J, Ahamad T, Alhokbany N, Majeed Khan MA, Arunachalam P, Amer MS, Alotaibi RM, Alshehri SM (2023) Reduced graphene oxide encapsulated perovskite-type lanthanum cobalt oxide nanoparticles for efficient electrolysis of water to oxygen reactions (OER/ORR). J Ind Eng Chem 121:100–106. https://doi.org/10.1016/J.JIEC.2023.01.011

58. Daiane Ferreira Da Silva C, Claudel F, Martin V, Chattot R, Abbou S, Kumar K, Jiménez-Morales I, Cavaliere S, Jones D, Rozière J, Solà-Hernandez L, Beauger C, Faustini M, Peron J, Gilles B, Encinas T, Piccolo L, Barros De Lima FH, Dubau L, Maillard F (2021) Oxygen evolution reaction activity and stability benchmarks for supported and unsupported IrOxElectrocatalysts. ACS Catal 11:4107–4116. https://doi.org/10.1021/ACSCATAL.0C04613/ASSET/IMAGES/LARGE/CS0C04613_0005.JPEG

59. Srinivasan S, Rathinam Y, Ganesan R, Alagarsamy A (2023) Construction of Fe2O3 nanoparticles decorated for a highly efficient oxygen evolution reaction activity. Energy Fuels 37:15976–15985. https://doi.org/10.1021/ACS.ENERGYFUELS.3C01672/ASSET/IMAGES/MEDIUM/EF3C01672_0010.GIF

60. Geng J, Kuai L, Kan E, Wang Q, Geng B (2015) Precious-metal-free Co–Fe–O/rGO synergetic electrocatalysts for oxygen evolution reaction by a facile hydrothermal route. ChemSusChem 8:659–664. https://doi.org/10.1002/CSSC.201403222

61. Alharbi FF, Gouadria SM, Alhawali L, Aman S, Farid HMT (2024) Perovskite nanostructure anchored on reduced graphene (rGO) nanosheets as an efficient electrocatalyst for oxygen evolution reaction (OER). Diamond and Related Materials, 148:111456, ISSN 0925–9635, https://doi.org/10.1016/j.diamond.2024.111456

62. Jo SG, Kim CS, Kim SJ, Lee JW (2021) Phase-controlled NiO nanoparticles on reduced graphene oxide as electrocatalysts for overall water splitting. Nanomaterials 11:3379. https://doi.org/10.3390/NANO11123379/S1

63. Shinde P, Rout CS, Late D, Tyagi PK, Singh MK (2021) Optimized performance of nickel in crystal-layered arrangement of NiFe2O4/rGO hybrid for high-performance oxygen evolution reaction. Int J Hydrogen Energy 46:2617–2629. https://doi.org/10.1016/J.IJHYDENE.2020.10.144

64. Zhang J, Li F, Chen W, Wang C, Cai D (2019) Facile synthesis of hollow Co3O4-embedded carbon/reduced graphene oxides nanocomposites for use as efficient electrocatalysts in oxygen evolution reaction. Electrochim Acta 300:123–130. https://doi.org/10.1016/J.ELECTACTA.2019.01.100

65. Zhao H, Chen C, Chen D, Saccoccio M, Wang J, Gao Y, Wan TH, Ciucci F (2015) Ba0.95La0.05FeO3−δ–multi-layer graphene as a low-cost and synergistic catalyst for oxygen evolution reaction. Carbon 90:122–129. https://doi.org/10.1016/J.CARBON.2015.04.013

66. Aziz SKT, Ummekar M, Karajagi I, Riyajuddin SK, Siddhartha KVR, Saini A, Potbhare A, Chaudhary RG, Vishal V, Ghosh PC, Dutta A (2022) A Janus cerium-doped bismuth oxide electrocatalyst for complete water splitting. Cell Rep. Phys Sci 3:101106. https://doi.org/10.1016/J.XCRP.2022.101106